THE JOURNAL OF PHYSICAL CHEMISTRY A

 VOLUME 106, NUMBER 49, DECEMBER 12, 2002

ARTICLES

Photodissociation Dynamics of Propiolic Acid at 193 nm: The State Distribution of the Nascent OH Product

Awadhesh Kumar,* Hari P. Upadhyaya, Prakash D. Naik, Dilip K. Maity, and Jai P. Mittal

Radiation Chemistry and Chemical Dynamics Division, Bhabha Atomic Research Centre, Mumbai 400 085, India

Received: July 8, 2002; In Final Form: September 25, 2002

Photolysis of propiolic acid (HC≡C−COOH) upon $\pi-\pi^*$ excitation at 193 nm leads to the C−O bond fission generating the primary product OH in a good yield. The partitioning of the available energy into the internal states and the translation of OH(v,J) is evaluated by measuring the relative intensities of ro-vibronic lines employing laser-induced fluorescence and their Doppler profiles, respectively. The vibrational distribution of nascent OH(v''=0 and 1) corresponds to the vibrational temperature of 1030 ± 80 K. The rotational population of OH(v''=0 and 1) is characterized by rotational temperatures of 800 ± 30 and 620 ± 30 K, respectively. Using widths of the Doppler-broadened lines, the OH(v''=0) average translational energy was measured to be 24.4 ± 3.0 kcal/mol, which implies about 75% of the total available energy goes to the translation of the fragments. The observed high translational energy is due to the presence of a barrier in the exit channel, suggesting the C−O bond cleavage occurs on an electronically excited potential energy surface. The measured partitioning of the available energy between the fragments OH and HCCCO is explained using the hybrid model with 37.5 kcal/mol of barrier in the exit channel. We employed ab initio molecular orbital theory to calculate structures and energetics of the ground and the excited electronic states of propiolic acid.

I. Introduction

Photodissociation of carboxylic acids is important for their role in atmospheric, combustion and interstellar chemistry. Acids are end products or important intermediates in the oxidation of hydrocarbons. Some of carboxylic acids such as HCOOH have been identified and some such as propiolic acid are expected to be present in the interstellar space.[1−3] Another interesting feature of carboxylic acid is their tendency to form hydrogen bonded dimers, and therefore are found as a mixture of monomers and dimers in the gas phase. Hence, thermodynamics, kinetics and spectroscopy of this class of molecules have been studied.[4]

UV laser induced photodissociation of carboxylic acids has gained importance in recent years,[5−11] primarily because it generates an atmospherically important OH radical. The OH can be produced either directly in a primary step by the C−O bond cleavage or in a secondary reaction via dissociation of the primary product HOCO formed after the C−C bond cleavage. The dynamics of dissociation leading to formation of OH can distinguish between these two mechanisms. In the reverse reaction to the C−O bond cleavage producing OH, a barrier is observed in some carboxylic acids.[10−12] Several workers have studied the photodissociation of carboxylic acids, and explored the dissociation dynamics by mapping the energy

* To whom correspondence should be addressed. E-mail: awadesh@apsara.barc.ernet.in.

10.1021/jp0215668 CCC: $22.00
Published on Web 11/15/2002

partitioning into the product states. Dissociation from the ground electronic state is known to lead to molecular elimination of CO_2 (reaction 1) or/and H_2O.

$$RCO_2H \rightarrow RH + CO_2 \quad (1)$$

Excitation to higher electronic states opens up radical channels, such as reactions 2 and 3, either from the initial excited state or the vibrationally hot ground electronic state after internal conversion.

$$RCO_2H \rightarrow RCO + OH \quad (2)$$

$$\rightarrow R + HOCO \quad (3)$$

Most of above studies on photodissociation are devoted to saturated carboxylic acids such as formic, acetic and trifluoroacetic acids, whereas literature is sparse on dissociation of unsaturated carboxylic acids. In the present work, we have investigated the dynamics of dissociation of propiolic acid (HC≡C−COOH) on irradiation by ArF laser at 193 nm under collisionless conditions. This work is in continuation of our earlier studies on photodissociation dynamics of saturated acids, such as acetic acid,[5] trifluoroacetic acid,[12] and unsaturated carboxylic acids, such as acrylic acid,[13] at 193 and/or 248 nm. Propiolic acid is not subjected to any study on its photophysics, and little is known about its photochemistry. Its He(II) photoelectron spectra are studied.[14] Besides its importance in atmospheric and combustion chemistry, propiolic acid (PA) is used in stereospecific synthesis.[15] Some metal propiolates are found to be energetic materials.[16] As PA is expected to be present in the interstellar space, its microwave spectroscopy is investigated in detail.[1−3,17] Theoretical calculations[2,18,19] predict the molecule to have planar geometry with the hydroxyl proton adopting cis (syn) or trans (anti) conformations with respect to the carboxyl group; the syn conformer being more stable by 3.6 kcal/mol with the rotational barrier of ∼6.4 kcal/mol. These calculations showed that its dipole moment originates almost entirely from the charge distribution of the COOH group implying that the degree of conjugation between the acetylenic and carbonyl groups is rather modest. Literature lacks high level ab initio molecular orbital (MO) calculations on this molecule.

In this work, the nascent product OH(v,J) formed on 193 nm photolysis of PA is monitored employing laser induced fluorescence (LIF) technique. We focused mainly on the partitioning of the available energy into various degrees of freedom of the photoproducts of the OH generating channel, and explored the possibility of existence of energy barrier in the exit channel.

II. Experimental Section

Propiolic acid (PA) is photolyzed at 193 nm and the nascent OH fragment is probed state selectively using LIF technique by exciting the (0,0) and (1,1) bands of the $A\ ^2\Sigma - X\ ^2\Pi$ system of OH and monitoring the total A−X fluorescence. The experimental set up for laser photolysis-laser-induced fluorescence (LP-LIF) is described elsewhere.[5] Briefly, the photolysis laser employed is an ArF excimer laser (Lambda Physik, Compex-102) operating at 193 nm. The probe beam is the second harmonic of the output of a dye laser (Quantel, TDL90) pumped by the second harmonic (532 nm) of a seeded Nd:YAG laser (Quantel, YG980 E-20). The dye laser operated with DCM special dye with the fundamental wavelength tuning range of 600 to 640 nm. The photolysis and the probe laser beams traverse orthogonally through two pairs of windows to intersect at the center of the reaction chamber, which is made of stainless steel and equipped with five arms and three ports for the pressure transducer, gas inlet, and the vacuum pump. Two orthogonal pairs of arms are provided with MgF_2 and quartz windows at the Brewster angle to facilitate transmission with reduced scattering of the photolysis and the probe beams, respectively. The fifth bottom arm is used to collect fluorescence with a lens (f = 50 mm) and to detect with a PMT (Hamamatsu, R 928P). A broadband-pass filter (λ_{center} = 310 nm, fwhm = 20 nm) is employed to cut off the scattered light from the photolysis laser. The fluorescence signal is integrated and averaged for 30 or 100 shots by a boxcar (SRS 250) and fed to a Pentium II PC, which controls the scan. The time delay (∼90 ns) between the photolysis and the probe lasers is controlled by a delay generator (SRS, DG535). Photodiodes are employed to monitor the energies of the photolysis and the probe beams to correct for the pulse-to-pulse fluctuation of the energy. The laser frequency was calibrated using an optogalvanic cell (Fe−Ne).

For all measurements, the PA vapor flows through the reaction chamber with a static pressure maintained at ∼25 mTorr, which is measured using a capacitance guage (Pfeiffer Vacuum). The product of pressure and the time delay being less than 3 Torr ns ensured that the OH state distribution is not affected by collisions. Both the laser beams were unfocused and their energies reduced substantially to avoid any multiphoton process and saturation by the photolysis and the probe lasers, respectively. The LIF intensity depends linearly on the pressure of propiolic acid around the pressure used in the experiments. This ensured a negligible contribution to the OH yield from the photodissociation of the dimer of propiolic acid. During irradiation the windows for the photolysis laser develop a thick coating from the deposits of some photoproducts, which were cleared regularly during the experiment to avoid the attenuation of the laser energy.

Excitation at 193 nm leads to fluorescence from the electronically excited PA. The fluorescence was dispersed with a monochromator (Jarrell Ash, model 82−410; resolution = 3 nm) and detected with the PMT. The signal was averaged for 300 shots at each wavelength and stored in a digital oscilloscope (LeCroy, 9350A) for further processing. PA (Fluka, >95% purity) was used as supplied after degassing and purification by several freeze−pump−thaw cycles.

III. Theoretical Calculations

Ab initio molecular electronic structure theories were employed to investigate the potential energy surface (PES) for OH dissociation channel in the ground as well as in the excited electronic states of PA accessible by 193 nm excitation. The ground-state full geometry optimization was carried out at the second-order Moller−Plesset (MP2) level of theory with 6-31+G(d,p) basis sets using Gaussian 92.[20] The geometry and energy were improved further through the calculations at Configuration Interaction (CI) level adopting the same sets of basis functions. For the ground-state fragments with odd electrons, the calculations were carried out at the restricted open shell HF (ROHF) level to eliminate any error due to spin contamination. Excited electronic state calculations were performed at the configuration interaction with single electronic excitation (CIS) level and excitation states of PA accessible (S_2 and T_5) using ArF laser at 193 nm were predicted from the vertical excitation energies. Each of the excited-state geometries (S_1, S_2, T_1-T_5) was then fully optimized following CIS procedure. Hessian calculations were performed with the final optimized geometries both in the ground and the excited states

to check the nature of the stationary geometries and to calculate the respective zero point energies. Orbitals participating in the electronic transitions were assigned for each of the excited states accessible with the respective fully optimized geometry using molecular density displaying program, MOLDEN.

IV. Results and Analysis

PA is expected to undergo multidissociation pathways from the ground and the excited electronic states. Three commonly observed dissociation channels (reactions 1−3, where R is HC≡C for PA) for carboxylic acids, in general, are also energetically favorable for PA. In addition, the C−H bond cleavage (reaction 4) and the molecular elimination of CO (reaction 5) are energetically possible dissociation channels.

$$HC{\equiv}C\ CO_2H \rightarrow C{\equiv}C\ CO_2H + H \qquad (4)$$

$$HC{\equiv}C\ CO_2H \rightarrow HC{\equiv}C{-}OH + CO \qquad (5)$$

We investigated dynamics of the C−O bond cleavage of PA producing OH (reaction 2) at 193 nm.

A. Formation of OH. Electronic absorption spectra of PA are not available in the literature. In general, the first absorption band of carboxylic acids lies below ∼260 nm, and is associated with the n−π* transition of the carbonyl group. The second band of acids is at ∼200 nm, which is associated with the $\pi-\pi$* transition. We recorded the UV absorption spectra of PA, which show three peaks at about 205, 198, and ≤190 nm. The wavelength at 193 nm excites the S_2 state of PA, via $\pi-\pi$* transition, from which it dissociates to yield OH in good yields. To understand the reason for the higher OH yields, we measured the absorption cross-section of PA (maintaining the pressure <80 mTorr) at 193 nm using a long path length cell (51 cm) and fast photodiodes. Assuming a negligible contribution from the dimers of PA at the low pressures used, we measured the absorption cross-section of PA at 193 nm to be 1.1×10^{-17} cm^2 molecule^{-1}. Thus, the high value of the absorption cross-section of PA at 193 nm coupled with probably a high quantum yield for the OH formation is responsible for the high yields of OH. The possibility of the high quantum yield for OH is supported by very small yields of the stable product C_2H_2 (reaction 1) measured with a FT-IR spectrometer. Thus, decarboxylation channel, a dominant dissociation channel from the ground electronic state of carboxylic acids in general, occurs to a small extent in photodissociation of PA at 193 nm. We obtained an indirect evidence for formation of HC≡C, which suggests that reaction 3 also takes place on excitation of PA at 193 nm (discussed in section D).

The $P_1(2)$ rotational line of the (0,0) band of the A−X system was detected using LIF to follow the formation of OH in real time by changing the time delay between the photolysis and the probe lasers. The growth of OH is fit to a single-exponential function (shown in Figure 1) with a unimolecular rate coefficient of 2×10^6 s^{-1}.

B. Nascent OH Distribution. The nascent photoproduct OH(v,J) was detected by LIF. Figure 2 shows the fluorescence excitation spectra of the (0,0) and (1,1) bands of the A $^2\Sigma^+$−X $^2\Pi$ system of OH. The OH line positions were assigned after ref 21. We use the standard notation $\Delta J(N'')$ for the transition and denote transitions associated with the spin−orbit states X $^2\Pi_{3/2}$ and A $^2\Pi_{1/2}$ with subscripts "1" and "2", respectively. The spectra show insignificant vibrational excitation with the most of OH generated in the vibrational ground state. Line intensity was normalized appropriately to extract information

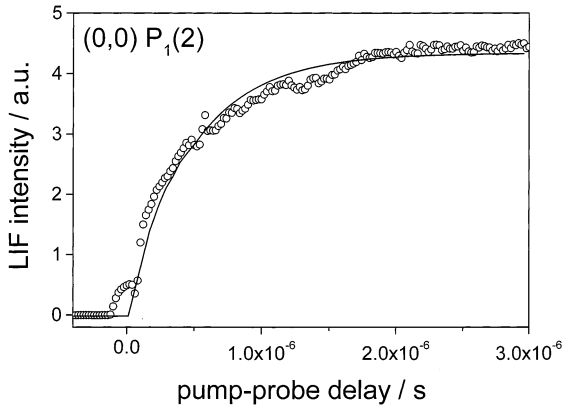

Figure 1. The time evolution of OH, probed by (0,0) P_1 (2) rotational line, produced from photodissociation of propiolic acid at 193 nm, and its fit to a single-exponential function with a unimolecular rate coefficient of 2×10^6 s^{-1}.

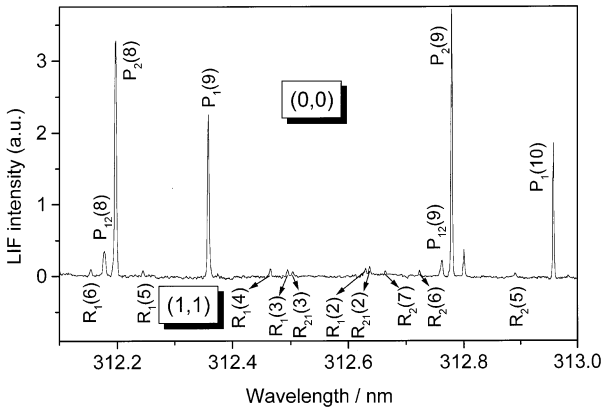

Figure 2. The figure shows a portion of the fluorescence excitation spectra (at 90 ns delay) of the (0,0) and (1,1) bands of the A $^2\Sigma^+$−X $^2\Pi$ system of OH generated from photodissociation of propiolic acid (∼25 mTorr) at 193 nm.

on the rotational and vibrational temperature from the corrected relative intensities.

1. Rotational Temperature. The rotational lines of the (0,0) band of OH were measured up to $N'' = 15$. Each rotational line was fitted to a Gaussian function and its area was evaluated. The measured area was corrected for the Einstein absorption coefficients (taken from ref 22), and energies of the photolysis and the probe lasers. The rotational population at J'', $P(J'')$, is proportional to the corrected line intensity, and is given by the Boltzmann equation,

$$\ln(P(J'')/(2J''+1)) = -\epsilon hc/kT_R + \text{constant} \qquad (6)$$

Except for lower N'', a plot of this eq 6 is a straight line (depicted in Figure 3), whose slope gives the rotational temperature, $T_R = 800 \pm 30$ K. Only $P_1(N'')$ and $P_2(N'')$ rotational lines were used for calculating T_R, because these lines were mostly free from interference from other lines. At lower N'' values, the rotational population is non-Boltzmann, and hence, these data are excluded from a Boltzmann fit to estimate T_R.

The rotational lines of the (1,1) band of OH were measured up to $N'' = 8$, and all the lines were used to calculate the rotational temperature after appropriate corrections to the measured area. A Boltzmann plot for rotational state distributions of OH(v''=1) is shown in Figure 3, with a T_R of 620± 30 K.

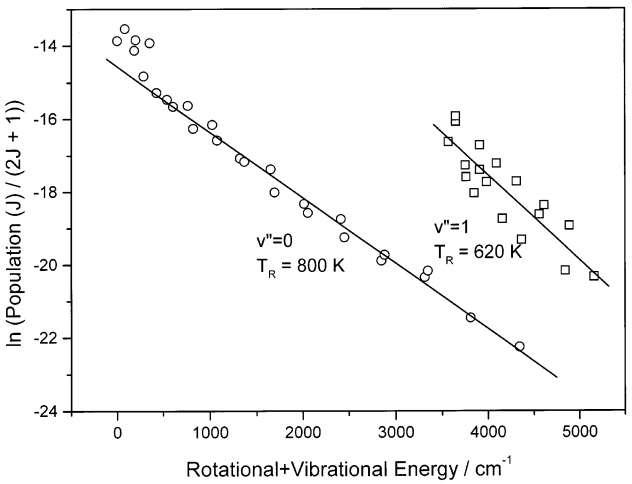

Figure 3. The figure depicts the Boltzmann plots for rotational state distributions of OH(v''=0 and 1) with the rotational temperature, T_R = 800 ± 30 and 620 ± 30 K, respectively, for the $v'' = 0$ and 1. At lower N'', the distribution in the $v'' = 0$ level is nonstatistical.

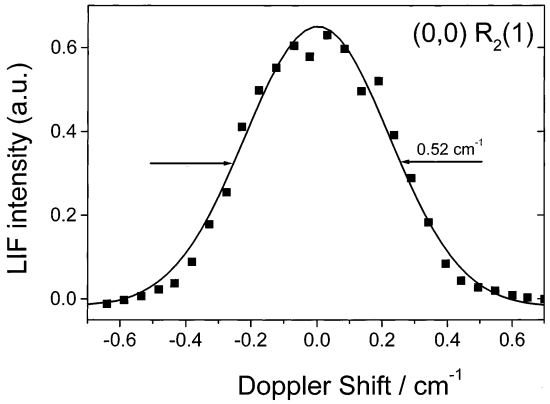

Figure 4. This figure shows a typical Doppler-broadened $R_2(1)$ line of the A $^2\Sigma^+ - X\ ^2\Pi$ (0,0) system of OH.

2. Vibrational Temperature. Assuming a Boltzmann distribution, a vibrational temperature can be obtained from the ratio of the LIF intensities of the same rotational line of the (0,0) and (1,1) transitions by

$$I(R_{1,2}(N'');v''=1)/I(R_{1,2}(N'');v''=0) = \exp(-\Delta\epsilon_v hc/kT_V) \quad (7)$$

where $\Delta\epsilon_v$ is the energy difference between $v'' = 1$ and $v'' = 0$ for a given spin−orbit state and N'', and T_V is the vibrational temperature. The constants h, c, and k have their usual meanings. Intensities of a few rotational lines P_1 (1), P_1 (2), Q_1 (5), and Q_1 (6) were used to estimate the T_V, and the average value for T_V was calculated to be 1030 ± 80 K.

3. Translational Temperature. The average translational energy of the photoproduct OH can be estimated using widths of Doppler-broadened rotational lines. The width is determined by the fragment molecular velocity, laser line width, and the thermal motion of the parent molecule. The laser line width being small (fwhm = 0.06 cm^{-1}), it was possible to deconvolute the width with the instrumental function (0.07 cm^{-1}), which was measured by the line width of thermalized OH at high pressure (50 Torr of ~0.1% PA in Ar) and longer delay time (115 μs). A typical Doppler-broadened line is shown in Figure 4. A few rotational lines were fitted to a Gaussian function, and their widths (fwhm), $\Delta\nu$, after deconvolution were used to calculate the translational temperature T_T using the Doppler relation

$$\Delta\nu = 7.16 \times 10^{-7}(T_T/m)^{1/2}\nu_0 \quad (8)$$

where m is the mass of the fragment OH. The average translational energy channeled into OH was estimated to be 24.4 kcal/mol from the average T_T.

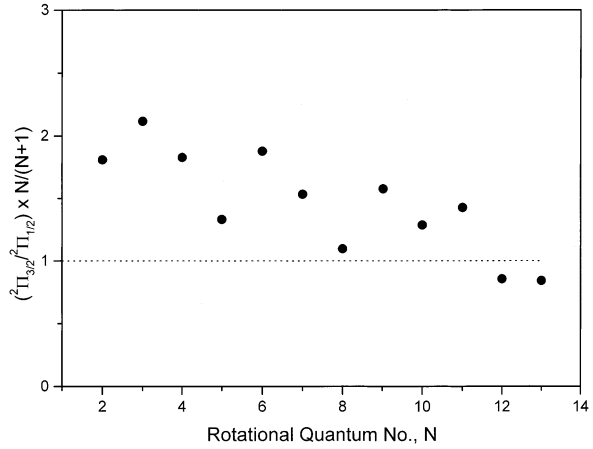

Figure 5. A plot of the relative populations of $^2\Pi_{3/2}$ to $^2\Pi_{1/2}$ states of the product OH against rotational quantum number N''.

4. Spin−Orbit State Population. The ground electronic state of OH being $^2\Pi$, there are two spin−orbit components $^2\Pi_{3/2}$ and $^2\Pi_{1/2}$. The relative populations, duly corrected, of $^2\Pi_{3/2}$ to $^2\Pi_{1/2}$ states of the product OH is plotted against N'' (depicted in Figure 5). The LIF intensities of only $P_{1,2}(N'')$ lines are used to obtain the spin−orbit population. The figure shows the distribution of OH population in two spin−orbit states to be nonstatistical at lower N'' with a small preference for $^2\Pi_{3/2}$. At higher N'', the ratio becomes statistical with value 1.

C. Theoretical Results. The present calculation at the second-order Moller−Plesset (MP2) level with 6-31+G(d,p) sets of basis functions predicts the most stable geometry for the ground electronic state S_0 to be planar with syn configuration for HOCO; the syn conformer being more stable than the anti by 3.9 kcal/mol. We calculated the transition state (TS) structure involved in the conversion of the syn to the anti conformer with the rotational barrier of 11.4 kcal/mol. The semiempirical method[18] calculates the relative stability and the rotational barrier to be respectively 3.6 and 6.4 kcal/mol. The present ab initio bond dissociation energy of the C−O bond of PA is calculated to be 104.5 kcal/mol in good agreement with the estimated value of 106.1 kcal/mol.[29] We calculated the TS structure for the C−C bond cleavage from the S_0 state of PA to explore the possibility of the secondary OH formation from the primary product HOCO. The barrier for the forward and the reverse reaction was calculated to be 135.9 and 5.2 kcal/mol, respectively.

Structures of PA in different excited electronic states are optimized at the configuration interaction with single electronic excitation (CIS) level, and the zero point energy corrected excitation energies are calculated to be 4.71 and 5.56 eV for the singlet states S_1 and S_2, respectively, and 2.39, 4.07, 4.57, 5.63, 5.82, and 7.25 eV for the triplet states T_1, T_2, T_3, T_4, T_5, and T_6, respectively. The optimized structure of the S_2 state (shown in Figure 6) has a nonplanar geometry with the plane of HOCO at an angle of 88° with respect to the plane of the carbon backbone of the molecule. The H−C≡C−C backbone in S_0 is changed to H−C═C−C in S_2. Thus, the S_2 minimum involves $^1\pi-\pi^*$ transition of the C≡C bond. Similar conclusion

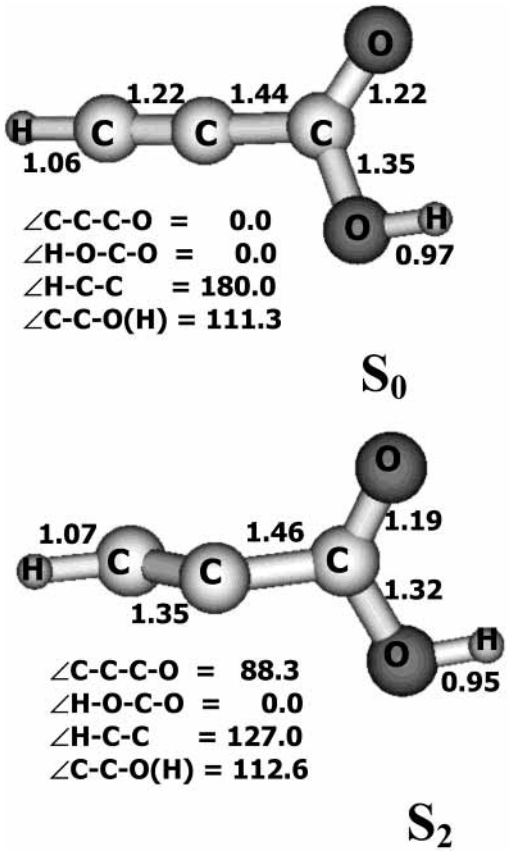

Figure 6. The optimized geometries of the S_0 and S_2 states of propiolic acid (details in the text); bond distances are in angstrom and the angles in degrees.

was drawn from analysis of molecular orbitals, which suggest $\pi_{C\equiv C}/\pi_{C=O}-\pi^*_{C\equiv C}$ transition for the S_2 state. The S_1 state involves $\pi_{C\equiv C}/n_{O(C=O)}-\pi^*_{C\equiv C/C=O}$ transition. Two lower triplet states T_1 and T_2 involve transitions similar to that of S_2 and S_1 states, respectively. The next two higher triplet states T_3 and T_4 involve mainly $\pi_{C\equiv C}/n_{O(C=O)}-\pi^*_{C\equiv C/C=O}$ transition with some contribution from $\pi_{C\equiv C}/n_{O(C=O)}-\pi^*_{C\equiv C-C=O}$ transition. The state T_5 involves mainly $\pi_{C\equiv C-C=O}$ $-\pi^*_{C\equiv C/C=O}$ transition with some contribution from $\pi_{C\equiv C/C=O}-\pi^*_{C\equiv C-C=O}$ transition. But, the triplet state T_6 involves mainly $\pi_{C=O}/n_{O(OH)}-\pi^*_{C\equiv C/C=O}$ transition with some contribution from $\pi_{C=O}/n_{O(OH)}-\pi^*_{C\equiv C-C=O}$ and $\pi_{C=O}/n_{O(OH)}-$Rydberg(29) transitions.

The Initial excitation at 193 nm leads to population of PA in S_2, from which it can dissociate to generate OH after the C−O bond cleavage. Several unsuccessful attempts were made to calculate the transition state structure responsible for OH from the S_2 electronic state both from the entrance and the exit channels. Probably, the excited molecule in S_2 crosses over to another nearby state(s) from which it dissociates. We also failed to calculate the TS structure for the OH channel from other electronic states. Ab initio MO calculation at higher level of the excited state CASSCF theory can probably be helpful in characterizing the TS structure of the OH forming channel.

D. Fluorescence. Fluorescence was observed between 250 and 600 nm after excitation of PA with ArF laser at 193 nm. The dispersed fluorescence spectrum (shown in Figure 7) at 150 ns delay has three distinct peaks at about 314, 440, and 490 nm, with a small peak at ∼285 nm. The fluorescence intensity at each peak wavelength is measured at almost the highest energy of the photolysis laser up to which linear dependence of the intensity with the energy is observed. The decay of fluorescence at peak wavelengths 314 and 440 nm is

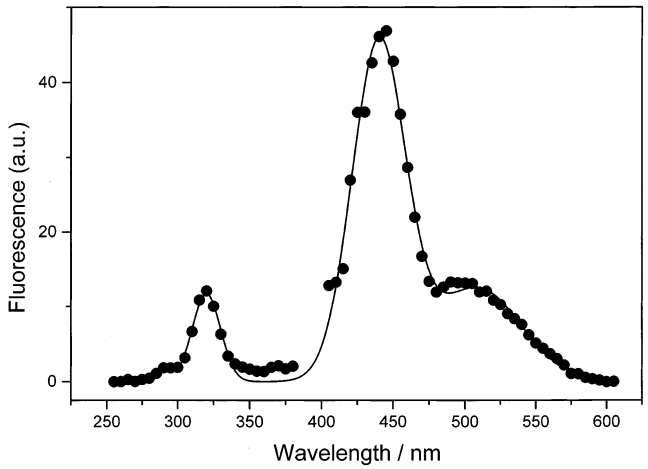

Figure 7. The figure depicts the dispersed fluorescence spectrum at 150 ns delay with three distinct peaks at about 314, 440, and 490 nm, with a small peak at ∼285 nm, resulting from the photoexcitation of propiolic acid at 193 nm.

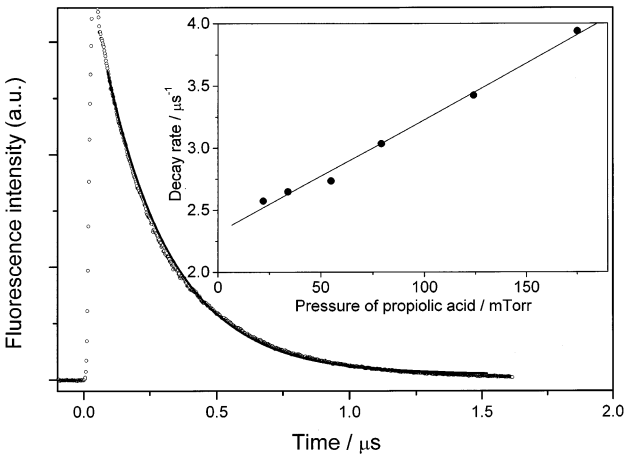

Figure 8. A typical observed fluorescence temporal profile (experimental points shown as empty circles) at 440 nm after irradiation of PA (175 mTorr) at 193 nm with a single-exponential fit (solid line, decay rate = 3.9 μs^{-1}) of its decay. The plot in the inset depicts the linear dependence of the fluorescence decay rates on varied pressures of PA.

TABLE 1: Measured Life Times and Quenching Rate Coefficients with Propiolic Acid of the Fluorescence Emitting States after its Irradiation at 193 nm

wavelength/nm	lifetimes/ns	quenching rate coefficient/ $cm^3\,molecule^{-1}\,s^{-1}$
315	330 ± 25	$(9.2 \pm 0.2) \times 10^{-10}$
440	430 ± 30	$(2.8 \pm 0.2) \times 10^{-10}$
490	120 ± 20	$(1.6 \pm 0.1) \times 10^{-10}$
	1400 ± 100	$(2.5 \pm 0.2) \times 10^{-10}$

single exponential; that at 490 nm is a better fit to a double exponential function. The dependence of fluorescence decay on the pressure of PA is studied to measure the quenching rate coefficients and the natural lifetimes of the emitting states at three peak wavelengths; these values are reported in Table 1. Figure 8 shows a typical temporal profile of fluorescence at 440 nm after irradiation of PA (175 mTorr) at 193 nm with a single-exponential fit of its decay. The plot in the inset depicts the linear dependence of the fluorescence decay rates on varied pressures of PA. Using the slope and the intercept of the linear plot, the quenching rate coefficient and the natural lifetime respectively are calculated. The quenching of fluorescence by

PA is quite efficient as inferred from observed high quenching rate coefficients (Table 1).

The electronic states of PA are known neither experimentally nor theoretically. Hence, the assignment of fluorescence cannot be made conclusively. The observed fluorescence between 250 and 450 nm is almost similar (with respect to the position of λ_{max}) to that of acrylic acid[13] after irradiation at 193 nm. On the bases of recent ab initio theoretical calculations,[23,24] the fluorescence observed[13] from acrylic acid with λ_{max} 285 and 314 nm is attributed to the S_2-S_0 transition, and that with λ_{max} at 440 nm due to the S_2-S_1 or the S_2-T_1 transition of acrylic acid. On the bases of the fluorescence assignment of acrylic acid and our theoretical calculations on PA, fluorescence in the region of 250 to 450 nm can be assigned to originate from the initially populated state, S_2 of PA. Thus, the emission with peaks at 285 and 315 nm can be assigned to the S_2-S_0 transition, and that at 440 nm can be attributed to the S_2-T_1/S_1 transition. Although the S_2 state of PA is assigned tentatively to be the emitting state, the radiative lifetime of the latter (~380 ns) cannot be supported by the high absorption cross-section (10^{-17} cm^2 $molecule^{-1}$, which corresponds to the natural lifetime of ~20 ns) measured for the S_2-S_0 transition of PA at 193 nm. These results suggest that the directly excited S_2 state of PA cannot be the emitter; the molecule undergoes rapid nonradiative decay to other secondary state(s). This secondary state can emit to explain the observed emission. Additionally, this state can dissociate or couple to another state to generate OH. Further work, both experimental and theoretical at high level, is required to assign unambiguously the emission from PA after excitation at 193 nm.

The decay of fluorescence at the peak 490 nm is double exponential implying contribution from different species. The slow component with lifetime of 1400 ± 100 ns can probably be assigned to the T_1-S_0 transition of PA. The fast component with lifetime of 120 ± 20 ns is ascribed to the Swan band transition of C_2. The measured radiative lifetime for the upper state of the Swan band transition (d $^3\Pi_g$ state) agrees with the literature values of 92−106 ns[25] and 120 ± 10 ns.[26] Even the quenching rate coefficient (1.6 ± 0.1) × 10^{-10} cm^3 $molecule^{-1}$ s^{-1} of fluorescence by PA is in good agreement with that of C_2 (d $^3\Pi_g$ state) by acetylene (1.2×10^{-10} cm^3 $molecule^{-1}$ s^{-1}) and ethylene (1.5×10^{-10} cm^3 $molecule^{-1}$ s^{-1}).[25]

The excited state of C_2 can be produced as a secondary product from the photoproduct C≡CH,[27,28] which is generated either as a primary product from the C−C bond cleavage (reaction 3, R is HC≡C) of PA, or as a secondary product from HC≡CCO (primary product of the C−O bond cleavage of PA, i.e., reaction 2) after it decays to give CO as a coproduct. To understand the feasibility of C≡CH formation after CO elimination from HC≡CCO we calculated the TS structure for this reaction, which gives an activation barrier of 42.5 kcal/mol, in good agreement with the prediction of 45.8 kcal/mol.[28] Thus, in our experiment with the total available energy of only 42.7 kcal/mol the decay of HC≡CCO to produce C≡CH and CO is not possible. Hence, C_2 (d $^3\Pi_g$ state) is generated in photolysis of PA at 193 nm from the primary product C≡CH. However, some contribution to the C_2 emission originating from two-photon absorption of PA at 193 nm cannot be ruled out as the emission was measured at high energy of the photolysis laser.

E. Product Energy Distribution. The available energy E_{avl} represents the energy remaining after the dissociation, which can be partitioned among various degrees of freedom of the primary photoproducts. E_{avl} is defined as the sum of the photon energy and the internal energy of the parent molecule minus the bond dissociation energy. Thus, E_{avl} of the primary photoproducts OH and HC≡CCO, E_{avl} (OH + HC≡CCO), is given by

$$E_{avl}(\mathrm{OH+HC{\equiv}CCO}) = h\nu(193\ \mathrm{nm}) + E_{int}(\mathrm{PA}) - D_0(\mathrm{HCCCO-OH}) \quad (9)$$

The energy of the photon $h\nu$ (193 nm) is 619 kJ/mol (147.9 kcal/mol). At room temperature, the parent PA molecules have on the average 3/2 RT = 0.9 kcal/mol rotational energy plus a small amount of energy distributed among the 15 normal modes of PA. We estimated the bond dissociation energy D_0 (HCCCO−OH) to be 106.1 kcal/mol using standard heats of formations ΔH_f^0.[29] Thus, the value of E_{avl} is 42.7 kcal/mol, which is partitioned among various degrees of freedom between the photofragments with $E_{avl} = E_{int}(\mathrm{OH}) + E_{int}(\mathrm{HC{\equiv}CCO}) + E_{trans}(\mathrm{OH+HC{\equiv}CCO})$, where E_{int} consists of both the rotational and vibrational excitation. The average rotational energy of the OH fragment, $\langle E_{rot}\rangle = 1.5 \pm 0.2$ kcal/mol, was obtained after summing over the rotational excitation in each populated vibrational state ($v'' = 0$ and 1),

$$\langle E_{rot}\rangle = \sum \langle E_{rot}\rangle_v = \sum P_v(J) E_{rot}(J) \quad (10)$$

where $P_v(J)$ is the state distribution and $E_{rot}(J)$ is the energy of a given rotational state J in $v'' = 0$ or 1. Similarly, the average vibrational energy was calculated to be ~0.1 kcal/mol using the vibrational distribution corresponding to the measured T_v of 1030 K. Thus, the average rotational and vibrational energy is $\langle E_{int}(\mathrm{OH})\rangle = 1.6$ kcal/mol. From the Doppler profile, the average translational energy in OH is 24.4 kcal/mol, which implies that of the fragment pair, $\langle E_{trans}(\mathrm{OH+HC{\equiv}CCO})\rangle$, to be 32.2 kcal/mol. These results are summarized in Table 2. Thus, the remaining available energy 8.9 kcal/mol, which is about 21% of the total energy, is channeled into the internal energy of the coproduct HC≡CCO, $\langle E_{int}$ (HC≡CCO)$\rangle$.

TABLE 2: The Partitioning of the Available Energy[a] into Translation and Internal Modes of the Photofragments (OH and HC≡CCO) of Propiolic Acid at 193 nm

	observed	statistical	impulsive	hybrid[b]
$\langle E_{trans}(\mathrm{OH+HC{\equiv}CCO})\rangle$	32.2	6.6	22.8	32.2
$\langle E_r(\mathrm{OH})\rangle$	1.5	2.3	1.0	1.8
$\langle E_v(\mathrm{OH})\rangle$	0.1	1.0	0.1	0.0
$\langle E_{int}(\mathrm{HC{\equiv}CCO})\rangle$	8.9	32.8	18.8	8.7

[a] All energies are in kcal/mol. $E_{avl} = 42.7$ kcal/mol. [b] Assuming an exit barrier of 37.5 kcal/mol.

V. Discussion

A. Energy Partitioning. The major fraction of the available energy is channeled into the translational energy of the photofragments, which can result from either the impulsive dissociation of the HCCCO−OH bond or the presence of an exit barrier. Because an impulsive dissociation occurs from a repulsive PES with high dissociation rate coefficient, in the present case with slow formation of OH, the molecule does not dissociate impulsively from the initially excited S_2 state. However, the parent molecule can dissociate after crossing over to another repulsive state, and thus explaining qualitatively a high fraction of the available energy being partitioned into the translational energy of the products. Alternatively, there can be an exit barrier to the C−O bond cleavage. Such an exit barrier is observed for a simple bond cleavage leading to OH in photodissociation of acetic[5,10] and acrylic acids.[11,13]

The results of partitioning of the available energy among various degrees of freedom of the two photofragments can be examined qualitatively in terms of two limiting models, the impulsive[30] and the statistical.[31] Although the impulsive model favors usually high translational fragment energy, it cannot explain the observed slow formation of OH from the S_2 state in the present work, as discussed earlier; another secondary state can be dissociative involving the impulsive mechanism. The observed Boltzmann distributions of the rotational and vibrational state distributions of OH(v,J) suggest the statistical nature of the fragment state distribution. However, the statistical model assumes a complete randomization of E_{avl} among all the degrees of freedom prior to dissociation. In the present work, probably a complete randomization of energy has not taken place since the vibration, rotation, and translation of OH have significantly different temperatures.

For quantitative prediction, we employed both statistical and impulsive models to calculate partitioning of the available energy of 42.7 kcal/mol into various degrees of freedom of photofragments OH and HC≡CCO. The structures of the ground and several excited electronic states of PA along with the photofragments OH and HC≡CCO were calculated using Gaussian92 at the MP2/6-31+G(d,p) level. The statistical model is based on the assumption that all possible combinations of product states are equally probable under the constraint of conservation of energy. We calculated vibrational frequencies and the rotational constants of the fragments at the MP2/6-31+G(d,p) level to estimate the density of states. This model, results shown in Table 2, very much underestimates the available energy appearing as the relative kinetic energy of the products, and overestimates the internal energy of HC≡CCO, and thus fails to explain the observed partitioning of the available energy among photofragments. The other limiting model, impulsive model, is based on the assumption that the amount of available energy acts as a repulsive potential along the breaking bond. The conservation of linear and angular momenta determines the energy partitioning among fragments. Like the statistical model, the impulsive model is also unable to explain well the measured data on energy partitioning between fragments. Both these models predict low rotational and vibrational energy going into OH as observed. But in contrast to the measured distribution, both predict low translational and high internal energy going into products. However, the prediction based on the impulsive model is relatively closer to the experimental values (Table 2).

The failure of both the statistical and impulsive models in explaining the partitioning of the available energy prompted us to apply the hybrid model,[32,33] comprising of both the impulsive and the statistical models. In this model the E_{avl} for the products is divided into the excess energy above the transition state and the energy released by the exit barrier, for which the partitioning of the available energy is treated respectively by the statistical and impulsive models. The energy partitioned to each fragment is obtained by adding contributions from each of these two models. The measured energy into fragments is reproduced well with an assumed exit barrier of 37.5 kcal/mol. This model predicts almost no vibrational excitation of OH.

The origin of a barrier in the exit channel of the C−O bond cleavage of a carboxylic acid can be due to dissociation from its enol form or to some features, such as nonadiabatic surface crossing, of the excited-state potential energy surfaces (PES).[9] In the absence of an α-H atom to the keto group of PA, its enol form does not exist. Thus, the surface crossing of the excited PES to which PA is excited initially should be mainly responsible for a high exit barrier of 37.5 kcal/mol. To fully understand the photodissociation dynamics of PA more experiments and high level of ab initio potential energy surfaces are necessary.

B. Dissociative State of Propiolic Acid. The excitation of PA at 193 nm populates the S_2 excited electronic state through the $^1(\pi,\pi^*)$ transition, similar to acrylic acid.[23,24] The excited molecule can relax through radiative decay, nonradiative decay or can undergo photodissociation. The relative importance of these relaxation processes depends on their relative rate coefficients. The slow formation of OH suggests that other radiative and nonradiative processes can compete with dissociation. Thus, the fluorescence (250−600 nm) from electronically excited PA could be observed. The short radiative lifetime (∼20 ns, estimated from the measured absorption cross section of PA at 193 nm) of S_2 with slow dissociation of PA forming OH precludes the initially excited S_2 state to be the dissociative state. Is this dissociative state the ground electronic state? It is suggested that after excitation of propynal[28] to high lying electronic states at 193 nm, internal conversion or intersystem conversion precedes the dissociation process. Dissociation of PA after excitation at 193 nm is expected to be similar to propynal. However, the C−O bond fission imparts a significant amount of energy into relative fragment translation indicating the presence of an exit barrier. This suggests that dissociation occurs on an electronically excited potential energy surface since a simple bond cleavage in the ground electronic state is generally barrierless.

Information on whether a molecule dissociates from a triplet potential energy surface can be obtained from the ratio of the spin−orbit states. A triplet dissociative state can change the spin−orbit ratio in the favor of the $^2\Pi_{3/2}$ state. Although there is some preference for the $^2\Pi_{3/2}$ state of OH produced after photolysis of PA at 193 nm, this alone is not sufficient to conclude unambiguously that PA dissociates from a triplet state.

The slow formation of OH can also result from the secondary dissociation of CO−OH, which is formed after the HCC−COOH bond cleavage. However, the energetics does not permit the secondary OH carrying away high translational energy of 26 kcal/mol. After the C−C bond cleavage (with the dissociation energy of ∼116 kcal/mol[29]) of PA, the available energy with HCC and HOCO fragments is about 32 kcal/mol. With the dissociation energy of the HO−CO bond cleavage of 36.0 kcal/mol,[29] HOCO will remain stable, and cannot channel the observed 21 kcal/mol of the translational energy into OH.

VI. Conclusions

The excitation of the S_2 state of PA with ArF laser at 193 nm leads to the C−O bond fission producing the primary product OH(v,J), which was state selectively detected employing LIF technique. The decarboxylation molecular channel, a major dissociation route of carboxylic acids from the ground electronic state, does not operate to a significant extent in this molecule. The partitioning of the available energy into the internal states and the translation of OH was evaluated by measuring the rovibronic lines and their Doppler profiles, respectively. Although the nascent OH is produced mostly in the $v'' = 0$, OH(v''=1) was also detected corresponding to the vibrational temperature of 1030 ± 80 K. The nascent population of OH(v''=0 and 1) is characterized by a rotational temperature of 800 ± 30 and 620 ± 30 K. Using widths of the Doppler-broadened lines, the OH average translational energy was measured to be 24.4 ± 3.0 kcal/mol. Thus, about 75% of the total available energy is channeled into relative fragment translation, suggesting the C−O bond fission has a barrier in the exit channel. This implies that

the dissociation occurs on an electronically excited potential energy surface since the simple bond fission in the ground electronic state is generally devoid of a barrier. To answer convincingly whether PA dissociates impulsively from a dissociative state or with an exit barrier, more experiments and theory at high level are needed, which can provide clear understanding of dynamics for OH formation on excitation of PA at 193 nm.

Acknowledgment. Authors acknowledge the constant support and suggestions from Drs A.V. Sapre and T. Mukherjee. Several valuable suggestions from referees are duly acknowledged.

References and Notes

(1) Wlodarczak, G.; Boucher, D.; Burie, J.; Demaison, J. *J. Mol. Spectrosc.* **1987**, *123*, 496.

(2) Lister, D. G.; Tyler, J. K. *Spectrochim. Acta A* **1972**, *28*, 1423.

(3) Watson, J. K. G. In *Vibrational Spectra and Structure*; During, J. R., Ed.; Elsevier: Amsterdam, 1977; Vol. 6.

(4) Hintze, P. E.; Aloisio, S.; Vaida, V. *Chem. Phys. Lett*. **2001**, *343*, 159 and references therein.

(5) Naik, P. D.; Upadhyaya, H. P.; Kumar, A.; Sapre, A. V.; Mittal, J. P. *Chem. Phys. Lett.* **2001**, *340*, 116.

(6) Kwon, H. T.; Shin, S. K.; Kim, S. K.; Kim, H. L.; Park, C. R. *J. Phys. Chem. A* **2001**, *105*, 6775.

(7) Su, H.; He, Y.; Kong, F.; Fang, W.; Liu, R. *J. Chem. Phys*. **2000**, *113*, 1891.

(8) Owrutsky, J. C.; Baronavski, A. P. *J. Chem. Phys*. **1999**, *111*, 7329.

(9) Arendt, M. F.; Browning, P. W.; Butler, L. J. *J. Chem. Phys*. **1995**, *103*, 5877.

(10) Hunnicutt, S. S.; Waits, L. D.; Guest, J. A. *J. Phys. Chem*. **1991**, *95*, 562.

(11) Kitchen, D. C.; Forde, N. R.; Butler, L. J. *J. Phys. Chem. A* **101**, *1997*, 6603.

(12) Naik, P. D.; Upadhyaya, H. P.; Kumar, A.; Sapre, A. V.; Mittal, J. P. Unpublished work.

(13) Upadhyaya, H. P.; Kumar, A.; Naik, P. D.; Sapre, A. V.; Mittal, J. P. *J. Chem. Phys*. In press.

(14) Von, W. N.; Bieri, G.; Schirmer, J.; Cederbaum, L. S. *Chem. Phys*. **1982**, *65*, 157.

(15) Ma, S.; Lu, X. *J. Chem. Soc*., *Chem. Commun*. **1990**, *22*, 1643.

(16) Stoner, Jr, C. E.; Brill, T. B. *Inorg. Chem*. **1989**, *28*, 4500.

(17) Davis, R. W.; Gerry, M. C. L. *J. Mol. Spectrosc*. **1976**, *59*, 407.

(18) Paoloni, L.; La-Manna, G. *J. Mol. Struct.* **1973**, *17*, 6568.

(19) Van, C. A.; Schaefer, L.; Siam, K.; Ewbank, J. D. *J. Mol. Struct.* (*Theochem)* **1989**, *56*, 271.

(20) Frisch, M. J.; Trucks, G. W.; Head-Gorden, M.; Gill, P. M. W.; Wong, M. W.; Foresman, J. B.; Johnson, B. G.; Schlegel, H. B.; Robb, M. A.; Replogle, E. S.; Gomperts, R.; Andres, J. L.; Rahavachari, K.; Binkley, J. S.; Gonzalez, C.; Martin, R. L.; Fox, D. J.; Defrees, D. J.; Baker, J.; Stewart, J. J. P.; Pople, J. A. *Gaussian 92*; Gaussian, Inc.: Pittsburgh, PA, 1992.

(21) Dieke, G. H.; Crosswhite, H. M. *J. Quant. Spectrosc. Radiat. Transfer* **1961**, *2*, 97.

(22) Chidsey, I. L.; Crosley, D. R. *J. Quant. Spectrosc. Radiat. Transfer* **1980**, *23*, 187.

(23) Fang, W.-H.; Liu, R.-Z. *J. Am. Chem. Soc*. **2000**, *122*, 10886.

(24) Fang, W.-H. *Chem. Phys. Lett.* **2000**, *325*, 683.

(25) Goldsmith, J. E. M.; Kearsley, D. T. B. *Appl. Phys. B* **1990**, *50*, 371 and references therein.

(26) Naulin, C.; Costes, M.; Dorthe, G. *Chem. Phys. Lett*. **1988**, *143*, 496 and references therein.

(27) Wodtke, A.; Lee, Y. T. *J. Phys. Chem*. **1985**, *89*, 4744.

(28) Haas, B.-M.; Minton, T. K.; Felder, P.; Huber, J. R. *J. Phys. Chem*. **1991**, *95*, 5149.

(29) The heats of formation (in kcal/mol) used to estimate the enthalpy of a reaction are ΔH_f^0(HC≡C−COOH) = −35.6 (estimated using the heats of formation of acrylic acid, propenal and propynal); ΔH_f^0(HC≡CCO) = 61.1, ΔH_f^0(HC≡C) = 134.3, ΔH_f^0(HC≡CCHO) = 25.8, and ΔH_f^0(H_2C=CHCHO) = −15.2 (from ref 28); ΔH_f^0(H_2C=CHCOOH) = −76.6 (from ref 10); ΔH_f0(CO) = −26.4, ΔH_f^0(OH) = 9.4; and ΔH_f^0(HOCO) = −53.3 (from Benson, S. W. *Thermochemical Kinetics*; John Wiley and Sons: New York, 1968).

(30) Tuck, A. F. *J. Chem. Soc., Faraday Trans. 2* **1977**, *73*, 689.

(31) Muckerman, J. T. *J. Phys. Chem*. **1989**, *93*, 179.

(32) North, S. W.; Blank, D. A.; Gezelter, J. D.; Longfellow, C. A.; Lee, Y.-T. *J. Chem. Phys.* **1995**, *102*, 4447.

(33) Chang, A. H. H.; Hwang, D. W.; Yang, X.-M.; Mebel, A. M.; Lin, S. H.; Lee, Y.-T. *J. Chem. Phys.* **1999**, *110*, 10810.